Simulation Modelling Practice and Theory 123 (2023) 102703

Contents lists available at ScienceDirect

Simulation Modelling Practice and Theory

journal homepage: www.elsevier.com/locate/simpat

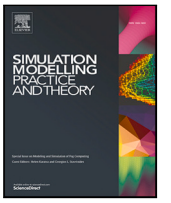

VTOL UAV digital twin for take-off, hovering and landing in different wind conditions☆

D. Aláez [a,*], X. Olaz [a], M. Prieto [a], J. Villadangos [a,b], J.J. Astrain [a,b]

[a] Mathematical Engineering and Computer Science Department, Universidad Pública de Navarra, Pamplona, 31006, Spain
[b] Institute of Smart Cities, Universidad Pública de Navarra, Pamplona, 31006, Spain

ARTICLE INFO

Keywords:
VTOL
UAV
Digital twin
Aerodynamic coefficients
Gazebo
Wind model

ABSTRACT

With UAVs becoming increasingly popular in the industry, vertical take-off and landing (VTOL) convertiplanes are emerging as a compromise between the advantages of planes and multicopters. Due to their large wing surface area, VTOL convertiplanes are subject to a strong wind dependence on critical phases such as take-off, landing, and hovering. Developing a new and improved unmanned aerial vehicle (UAV) is often expensive and associated with failures and accidents. This paper proposes the dynamic characterization of a commercial VTOL convertiplane UAV in copter mode and provides a novel method to estimate the aerodynamic forces and moments for any possible wind speed and direction. Starting from Euler's equations of rigid body dynamics, we have derived the mathematical formulation to precisely consider aerodynamic forces and moments caused by any wind speed and direction. This unique approach will allow for VTOL convertiplane UAVs to be trained and tested digitally in take-off, hovering, and landing maneuvers without the cost and hassle of physical testing, and the dependence on existing wind conditions. A digital twin of a VTOL convertiplane UAV in copter mode has been modeled and tested in the Gazebo robotics simulator. Take-off, hovering and landing maneuvers have been compared with and without the wind physics model. Finally, the simulator has been tested against real flight conditions (reproducing the mean wind speed and direction only), showing a natural and realistic behavior.

1. Introduction

Unmanned aerial vehicles (UAVs) are growing in use in the industry, especially for inspecting power lines, bridges, plants, buildings, facades, sewers, railways, and wind turbines [1].

Typically, there are three different conceptual UAV models: multicopter, plane, and VTOL (Vertical Take-Off and Landing) convertiplanes [2]. Convertiplane UAVs offer the combined advantages of copters and planes by being able to take off and land without the need of a runway, with a better flight efficiency for extended flight times than multicopters. Despite their advantages, convertiplane UAVs are very sensitive to wind conditions at the most critical stages of flight: take-off, landing, and hovering. When

☆ Funding: This work has been supported in part by the Ministerio de Ciencia e Innovación (Spain) under the research grant RTI2018-095499-B-C31 IoTrain; in part by Agencia Estatal de Investigación (AEI) and European Union NextGenerationEU/PRTR PLEC2021-007997: Holistic power lines predictive maintenance system; and in part by the Government of Navarre (Departamento de Desarrollo Económico) under the research grants 0011-1411-2021-000021 EMERAL: Emergency UAVs for long range operations, 0011-1365-2020-000078 DIVA, and 0011-1411-2021-000025 MOSIC: Plataforma logística de largo alcance, eléctrica y conectada.

* Corresponding author.
E-mail address: daniel.alaez@unavarra.es (D. Aláez).

https://doi.org/10.1016/j.simpat.2022.102703

Available online 28 November 2022

the copter mode is enabled, even slight crosswinds and gusts can significantly alter the UAV's attitude and position, increasing the risk of failure.

Safe operation is a critical issue [3]. Many inspection activities are classified as high-risk operations, and errors come at a high expense of time and money. In addition, the use of experimental technologies and designs often leads to failures and accidents, which can quickly elevate the development cost of a new or improved UAV. A trending way to reduce development costs is creating a high-fidelity model of the UAV from the conceptual design stage. By deploying this model in a digital environment, many aspects of the design and control can be tested or refined: aerodynamics, propulsion, flight control, structural integrity, etc.

Throughout this work, we propose a novel approach to completely model a VTOL convertiplane UAV during copter mode and simulate the aerodynamic effects of wind incoming from any direction.

2. Related works

2.1. Digital twins

The digital twin (DT) concept, understood as a virtual or digital equivalent of a physical product, was first introduced at the University of Michigan back in 2002 [4]. It contains three main parts:

- Physical products in real space.
- Virtual products in virtual space.
- The connections of data and information that tie the virtual and real products together.

In the following decade, many advances in quantity, richness, and fidelity [5] of recollected data have been developed, both by the physical product and its digital twin. Digital twins are of most use when an object is changing over time, thus making the initial model of the object invalid, and when measurement data that can be correlated with this change can be captured [6]. The ability to reproduce high-risk environments and specific situations without risking the aircraft is also advantageous. We can predict the aircraft behavior in an specific scenario and flight circumstances.

Efficient digital twins offer real-time simulation capabilities and visualization of complex systems, similar to the concept of *Hardware-in-the-loop* (HIL). This concept involves simultaneous control system loop testing within the software and the actual hardware environment, offering significant advantages such as real-time adjustment [7].

First HIL systems were produced for flight simulation [8]. Although this concept has been around for over 40 years, it has gained traction over the last 10 years, recently appearing on NASA aircraft and satellites roadmaps as the third most important technological development challenge [9]. Some VTOL HIL-related works have been proposed [10,11], but none of them consider arbitrary wind conditions.

A step below HIL simulation is software in the loop (SIL or SITL). It may be realized in the early stages of software development, offering the possibility to execute tests even before the hardware is available and thus detect errors [12].

2.2. UAV digital twins

Digital twins are powerful in the design and performance optimization stages of UAVs. In conventional simulators, the information is usually collected on-site, and then the UAV is optimized offline [13], leading to low development efficiency. Simulators have always been used as a UAV verification tool, but typically lack a proper integration of hardware and software [14].

A very popular open-source robotics operating system in DT modeling is ROS [15–17]. Its communication capabilities provide an standardized interface for custom plugin implementation.

In the physics simulation and visualization field, Gazebo is also gaining traction for robotic DTs [18,19]. It is also well integrated with ROS.

The Gazebo simulator [20] is a suitable simulation package. For UAV purposes, some features are missing. For example, only forward-flight aerodynamics can be modeled with the existing plugins, which is insufficient for VTOL convertiplanes. Other simulator alternatives (Airsim [21], Simulink [22], Unity [23]) neither provide a suitable solution.

When simulating UAV aerodynamics, the wind is assumed negligible compared to the forward-flying speed. It is only studied for pilot training [24], flight planning [25], and aeroelasticity phenomena [26]. In some cases, it can be taken into account by adding a drift angle [11]. These assumptions are valid in conventional aircraft and plane configurations, but not for VTOL convertiplanes. Omitting the effects of wind on a convertiplane in copter mode can cause significant deviations between the digital twin and the actual UAV [27].

To date, most UAV digital twins have been designed for quadcopters [12,14,28], where wind conditions can generally be neglected due to the lack of aerodynamic surfaces other than propellers.

2.3. Contributions

We have developed a novel mathematical model that allows us to estimate forces and moments acting on the whole UAV depending on the direction of the wind and the vehicle speed at any given moment.

We propose a digital twin of a commercial VTOL convertiplane UAV (from now on abbreviated as: VTOL-DT–VTOL Digital Twin) called Marvin, manufactured by FuVeX[1] (see Fig. 1).

[1] Fuvex website: https://www.fuvex.es/.

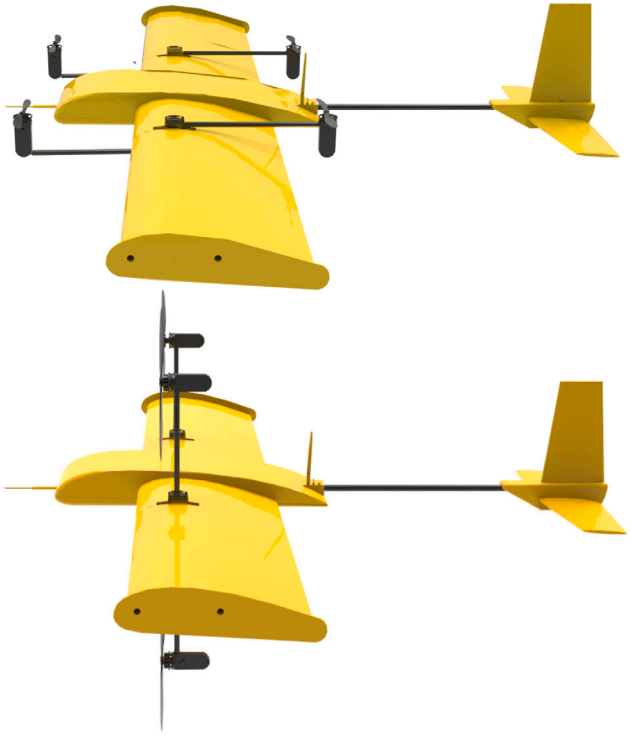

Fig. 1. 3D render of a Marvin UAV-VTOL in copter and plane mode.

The VTOL-DT is modeled mathematically considering: gravity, aerodynamic and propulsive contributions. It can simulate any arbitrary wind direction over the aircraft, relevant in vertical take-off, hovering, and landing conditions.

The VTOL-DT is characterized by ANSYS[2] computer fluid dynamics (CFD) simulations to a finite number of attitudes with respect to the wind, for which aerodynamic coefficients are obtained. We use a linear interpolation algorithm to estimate such coefficients in non-simulated conditions.

The physics simulator of our digital twin implements a custom aerodynamics plugin which integrates the mentioned aerodynamic coefficients.

The flight controller is part of the VTOL-DT. It is implemented using the same code as the real aircraft and executed as SITL, achieving virtually the same flight response as the real vehicle.

Finally, the VTOL-DT model is tested against real flight experiments in windy conditions, considering the measured mean wind speed and direction.

3. VTOL-DT modeling

The aircraft, manufactured by FuVeX, was chosen due to all the flight configurations available. This allows for a very rich and complete learning experience, where different proposals can be tested in complex environments and equally complex flight modes. It consists of a fixed wing, a conventional tail, and four electric motors mounted over a tilt mechanism. Depending on the selected flight mode, the tilt mechanism can turn the four motors from the vertical axis to a forward-flight position. Fig. 1 includes a schematic explanation of the tilt mechanism.

To model the aircraft's dynamics, three flight phases must be considered:

1. **Copter mode**: used by the actual UAV during take-off, landing, and hovering flight. All four motor axes are aligned with the vertical axis, and flight mechanics are controlled by conventional quadcopter models.
2. **Plane mode**: used during cruise flight, the motor axes are aligned with the forward flight direction. Flight control is obtained by a combination of torque and thrust differences between the four motors, plus the elevator and rudder input. The Marvin has no ailerons.

[2] https://www.ansys.com/.

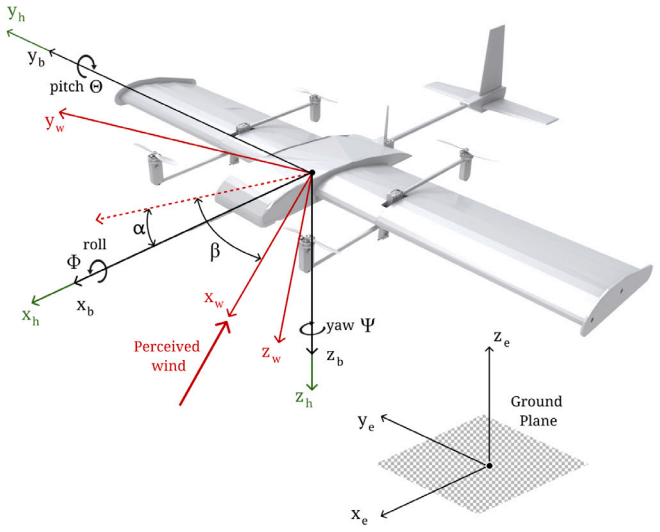

Fig. 2. Reference systems used in the mathematical model.

3. **Transition mode**: from copter to plane mode, and vice versa. The tilting mechanism progressively turns the axes of all 4 motors at once. This step is critical. In order to allow for this transition, flight speed must be higher than stall speed in plane mode: $\left|\vec{V}_{flight}\right| > \left|\vec{V}_{stall}\right|$.

As previously stated, only the copter mode is relevant for take-off, hover, and landing phases, where the wind effects are critical. Therefore, we will base our equations on this mode. This section aims to derive the mathematical formulation of the VTOL dynamics based on gravity, aerodynamic, and propulsion actions in copter mode. The use of a *perceived wind axes* coordinate system will simplify the description of the aerodynamic actions depending on the wind direction.

Fig. 2 contains a graphical description of the different reference systems and axes that will be used in the following section.

3.1. Mathematical model

The most generalized method for dynamic flight characterization in aeronautics is based on Euler angles. This procedure starts from Newton's Second Law of Motion, which relates force exerted to a body with its resulting acceleration:

$$\vec{F} = \frac{d(m\vec{V})}{dt}, \tag{1}$$

where m is the aircraft mass and $\vec{V}$ the absolute speed of the center of mass (CoM) in an inertial coordinate system. $\vec{F}$ is associated with external forces acting over the CoM. Similarly:

$$\vec{G} = \frac{d\vec{h}}{dt}, \tag{2}$$

$$\vec{h} = I\vec{w}, \tag{3}$$

where $\vec{G}$ is the resulting moment due to external forces around the CoM, $\vec{h}$ the total kinetic moment, I the aircraft's inertia tensor, and $\vec{w}$ its absolute angular speed around the CoM.

The inertia tensor is defined as a symmetric 3×3 matrix:

$$I = \begin{pmatrix} I_x & -J_{xy} & -J_{xz} \\ -J_{xy} & I_y & -J_{yz} \\ -J_{xz} & -J_{yz} & I_z \end{pmatrix}, \tag{4}$$

whose diagonal elements represent momentum over the given system, and the remaining elements are the products of inertia.

Next, we define the force, momentum, velocity and angular velocity vectors respectively, based on their components:

$$\vec{F} = (F_x, F_y, F_z)^T, \tag{5}$$

$$\vec{G} = (L, M, N)^T, \tag{6}$$

$$\vec{v} = (u, v, w)^T, \tag{7}$$

$$\vec{w} = (p, q, r)^T, \tag{8}$$

where F_x, F_y, F_z represent the forces on each axis; L, M, N the corresponding moments around x_b, y_b, z_b respectively; u, v, w are the corresponding linear velocities; and p, q, r the angular velocities referred to the same axis (see Fig. 2 for axis reference).

Given the time derivative of a vector in an inertial system, we need to add one extra term to express it in a body-axes reference frame: the cross product of the rotating system angular speed with respect to the inertial, multiplied by the vector to be derived. Thus, the momentum and kinetic moment theorems can be expressed as:

$$\vec{F} = m(\frac{\partial \vec{V}}{\partial t} + \vec{\omega} \times \vec{V}), \tag{9}$$

$$\vec{G} = \frac{\partial \vec{h}}{\partial t} + \vec{\omega} \times \vec{h}. \tag{10}$$

Manipulating and solving the expressions above, we obtain:

$$\begin{aligned} F_x &= m(\dot{u} - rv + qw), \\ F_y &= m(\dot{v} + ru - pw), \\ F_z &= m(\dot{w} - qu + pv), \\ L &= I_x\dot{p} - J_{xz}\dot{r} + (I_z - I_y)qr - J_{xz}pq, \\ M &= I_y\dot{q} - (I_z - I_x)pr + J_{xz}(p^2 - r^2), \\ N &= I_z\dot{r} - J_{xz}\dot{p} - (I_x - I_y)pq + J_{xz}qr. \end{aligned} \tag{11}$$

The given system of Eqs. (11) is commonly known as *Euler's motion equations for rigid body dynamics* [29]. As the name implies, the body is assumed to be one single rigid body, neglecting control surfaces' and other subsystems' associated degrees of freedom, and the kinetic moment with respect to rotating systems.

The next step is to particularize the external forces and momentum involved in this system. We will follow the formulation developed by [29], which subdivides them into:

- **Gravity actions**: in a local level system (LLS, denoted by superscript ^{h}), the expression only contains a term in the z axis:

$$\vec{F}_G^{\,h} = \begin{pmatrix} 0 \\ 0 \\ mg \end{pmatrix}, \tag{12}$$

  where g represents the acceleration due to gravity at a given point. To project this vector on a body-fixed system (BFS, denoted by superscript ^{b}), a rotation matrix has to be applied from LLS to BFS:

$$\vec{F}_G^{\,b} = \begin{pmatrix} F_{Gx} \\ F_{Gy} \\ F_{Gz} \end{pmatrix} = L_{bh}\vec{F}_G^{\,h} = \begin{pmatrix} -mg\ \sin\theta \\ mg\ \cos\theta\ \sin\phi \\ mg\ \cos\theta\ \cos\phi \end{pmatrix} \tag{13}$$

  where θ is the pitch angle, and ϕ the roll angle.
- **Aerodynamic actions**: external forces and moments due to aerodynamic effects.
- **Propulsive actions**: external forces and moments originated by propellers' rotation and combinations of them.

If the System of Eqs. (11) is further expanded, introducing and separating the components based on this scheme, the new system is:

$$\begin{aligned} -mg\ \sin\theta + \quad & F_{Tx} + F_{Ax} = m(\dot{u} - rv + qw), \\ mg\ \cos\theta\ \sin\phi + \quad & F_{Ty} + F_{Ay} = m(\dot{v} + ru - pw), \\ mg\ \cos\theta\ \cos\phi + \quad & F_{Tz} + F_{Az} = m(\dot{w} - qu + pv), \\ L_T + L_A = \ & I_x\dot{p} - J_{xz}\dot{r} + (I_z - I_y)qr - J_{xz}pq, \\ M_T + M_A = \ & I_y\dot{q} - (I_z - I_x)pr + J_{xz}(p^2 - r^2), \\ N_T + N_A = \ & I_z\dot{r} - J_{xz}\dot{p} - (I_x - I_y)pq + J_{xz}qr. \end{aligned} \tag{14}$$

Subscripts $_T$ and $_A$ refer to the propulsive actions and aerodynamic actions, respectively.

A common assumption in flight mechanics [30] consists of assuming the earth as flat and non-rotating, allowing us to consider the earth-fixed frame as inertial. This theory is known as the *Flat Earth Hypothesis*. A step-by-step demonstration of the omitted mathematical formulation can be found in [29]. Thanks to this assumption, the CoM trajectory can be obtained in an earth-fixed frame more easily.

3.2. Wind model

Once the generic Euler equations have been developed, the aerodynamic and propulsive terms have to be particularized for the VTOL UAV. In this case, for the copter flight setup, the wind speed is of a similar order to the flight speed, so this component cannot

be neglected. In fact, during hovering flight (or close to), the wind speed component will be the main component to which the flight controller will need to respond to keep the desired position and attitude. The greater surface area of a VTOL vehicle makes it more reactive to wind currents acting on its surface.

The absolute ground speed, in an earth-fixed frame (denoted by superscript ^{e}), is determined as the sum of the speed perceived by the aircraft, usually called true airspeed, and the wind speed:

$$\vec{V}^{e}_{ground} = \vec{V}^{e}_{perceived} + \vec{V}^{e}_{wind}. \tag{15}$$

Expanding all vectors component by component:

$$\vec{V}^{e}_{perceived} = \dot{x}^{e}\,\vec{i} + \dot{y}^{e}\,\vec{j} + \dot{z}^{e}\,\vec{k} - (u^{e}_{w}\,\vec{i} + v^{e}_{w}\,\vec{j} + w^{e}_{w}\,\vec{k}), \tag{16}$$

where $\dot{x}^{e}, \dot{y}^{e}, \dot{z}^{e}$ are the ground velocities of the CoM in an earth-fixed frame, and $u^{e}_{w}, v^{e}_{w}, w^{e}_{w}$ are the wind velocities.

The magnitude of velocity is calculated as follows:

$$\left|\vec{V}^{e}_{perceived}\right| = \sqrt{(\dot{x}^{e} - u^{e}_{w})^2 + (\dot{y}^{e} - v^{e}_{w})^2 + (\dot{z}^{e} - w^{e}_{w})^2} \tag{17}$$

If expressed in *perceived wind frame* (denoted by superscript ^{w}), the only remaining component is in the x axis, aligned with the wind direction:

$$\vec{V}^{\,w}_{perceived} = \begin{pmatrix} \sqrt{(\dot{x}^{e} - u^{e}_{w})^2 + (\dot{y}^{e} - v^{e}_{w})^2 + (\dot{z}^{e} - w^{e}_{w})^2} \\ 0 \\ 0 \end{pmatrix} \tag{18}$$

Thanks to this transformation, the remaining components disappear, allowing for more straightforward aerodynamic forces and moments calculation.

Next, the lift (L^{w}), drag (D^{w}), lateral force (Q^{w}), pitching moment (M^{w}_{A}), rolling moment (L^{w}_{A}) and yawing moment (N^{w}_{A}), respectively, can be calculated in a perceived wind reference frame with the commonly used expressions:

$$L^{w} = \frac{1}{2}\rho\left|\vec{V}^{e}_{perceived}\right|^2 S C_{L}(\phi,\theta,\psi), \tag{19}$$

$$D^{w} = \frac{1}{2}\rho\left|\vec{V}^{e}_{perceived}\right|^2 S C_{D}(\phi,\theta,\psi), \tag{20}$$

$$Q^{w} = \frac{1}{2}\rho\left|\vec{V}^{e}_{perceived}\right|^2 S C_{Q}(\phi,\theta,\psi), \tag{21}$$

$$M^{w}_{A} = \frac{1}{2}\rho\left|\vec{V}^{e}_{perceived}\right|^2 S\, c\, C_{M}(\phi,\theta,\psi), \tag{22}$$

$$L^{w}_{A} = \frac{1}{2}\rho\left|\vec{V}^{e}_{perceived}\right|^2 S\, c\, C_{LA}(\phi,\theta,\psi), \tag{23}$$

$$N^{w}_{A} = \frac{1}{2}\rho\left|\vec{V}^{e}_{perceived}\right|^2 S\, c\, C_{NA}(\phi,\theta,\psi), \tag{24}$$

where ρ is the air density, S is the reference surface area, and c is the reference wing chord length. Once the UAV's perceived velocity is known, the only unknowns in these equations are the respective force or moment coefficients ($C_{L}, C_{D}, C_{Q}, C_{M}, C_{LA}, C_{NA}$), as a function of roll (ϕ), pitch (θ) and yaw (ψ) angles. Those coefficients will have to be estimated via computational fluid dynamics (CFD) simulations.

Considering the UAV as a unique rigid body, only one coefficient for each term will need to be simulated for each incoming wind direction. Even so, the infinite possible attitude configurations will require a discretization of the domain, studied in the upcoming sections.

With the help of a rotation matrix, we can express the perceived wind frame forces and momentum in a body-fixed frame like (14):

$$\begin{pmatrix} F_{Ax} \\ F_{Ay} \\ F_{Az} \end{pmatrix} = L_{bw} \begin{pmatrix} -D^{w} \\ -Q^{w} \\ -L^{w} \end{pmatrix}, \tag{25}$$

where L_{bw} is the rotation matrix between perceived wind axes to body-fixed axes, equivalent to:

$$\begin{aligned} L_{wb} = L^{T}_{bw} &= \begin{pmatrix} \cos\alpha\cos\beta & \sin\beta & \sin\alpha\cos\beta \\ -\cos\alpha\sin\beta & \cos\beta & -\sin\alpha\sin\beta \\ -\sin\alpha & 0 & \cos\alpha \end{pmatrix}^{T} \\ &= \begin{pmatrix} \cos\alpha\cos\beta & -\cos\alpha\sin\beta & -\sin\alpha \\ \sin\beta & \cos\beta & 0 \\ \sin\alpha\cos\beta & -\sin\alpha\sin\beta & \cos\beta \end{pmatrix}, \end{aligned} \tag{26}$$

where α is the angle of attack of the perceived speed and β its drift angle [29]. Multiplying and expanding the product at (25), we arrive to:

$$\begin{aligned} F_{Ax} &= -D^w \cos\alpha \cos\beta + Q^w \cos\alpha \sin\beta + L^w \sin\alpha, \\ F_{Ay} &= -D^w \sin\beta - Q^w \cos\beta, \\ F_{Az} &= -D^w \sin\alpha \cos\beta + Q^w \sin\alpha \sin\beta - L^w \cos\beta. \end{aligned} \tag{27}$$

Analogously, aerodynamic moments can be determined as:

$$\begin{pmatrix} L_A \\ M_A \\ N_A \end{pmatrix} = L_{bw} \begin{pmatrix} L_A^w \\ M_A^w \\ N_A^w \end{pmatrix}, \tag{28}$$

obtaining:

$$\begin{aligned} L_A &= L_A^w \cos\alpha \cos\beta - M_A^w \cos\alpha \sin\beta - N_A^w \sin\alpha, \\ M_A &= L_A^w \sin\beta + M_A^w \cos\beta, \\ N_A &= L_A^w \sin\alpha \cos\beta - M_A^w \sin\alpha \sin\beta + N_A^w \cos\beta. \end{aligned} \tag{29}$$

This way, aerodynamic forces and moments are fully characterized. Lastly, to complete the mathematical model of copter flight, only propulsive actions remain to be determined.

3.3. Propulsion model

For this particular UAV, rear motors are on an upper plane than front motors, although this does not affect forces and torques modeling in copter mode. Force on the rotor direction for each motor can be modeled like [31]:

$$F_i = K_T \omega_i^2, \tag{30}$$

where K_T is a thrust constant dependant on the specific propeller used, ω_i is the angular speed of the ith rotor. Also, torque is modeled as:

$$\tau_i = b\,\omega_i^2 + I_M \dot{\omega}_i, \tag{31}$$

where b is referred to a torque constant dependant on the motor and propeller used, and I_M is the motor and propeller's inertia. Composing the force output of all four motors:

$$T = \sum_{i=1}^{4} F_i = K_T \sum_{i=1}^{4} \omega_i^2; \;\; \vec{T}^{\,b} = \begin{pmatrix} 0 \\ 0 \\ T \end{pmatrix}. \tag{32}$$

Different yaw, pitch, and roll actions are performed combining forces and torques produced by the four motors [32], following this scheme:

$$\begin{aligned} L_T &= (F_{FL} + F_{BL} - F_{BR} - F_{FR})\, w, \\ M_T &= (F_{FL} - F_{BL} - F_{BR} + F_{FR})\, l, \\ N_T &= (\tau_{FL} + \tau_{BL} + \tau_{BR} + \tau_{FR}), \end{aligned} \tag{33}$$

where L_T, M_T, N_T are the rolling moment, pitching moment, and yawing moment in body frame, caused by the propulsive actions. A complete diagram of forces and torques over the UAV is shown in Fig. 3.

Subindices $_F$, $_B$, $_L$, $_R$ denote front, rear, left and right, respectively. Two distances w and l have also been defined, referred to the separation between a motor and the midplane of the aircraft, and the half-length separating two motors of the same side, respectively.

With this, every term on the System of Eqs. (14) is fully defined. For any given initial conditions and control inputs, such as motor input, with the help of an appropriate time integrator, we can estimate the position and attitude of the aircraft at any given time step.

4. Aerodynamic coefficients characterization

Once the propulsive, gravity, and aerodynamic actions have been modeled, the next step is to evaluate the aerodynamics. From equations obtained in Section 3.1, we derived the need to estimate force and torque coefficients, respect to wind axes, for a wide range of angle combinations. For this task, ANSYS Fluent RANS (*Reynolds-averaged Navier–Stokes*) simulations have been performed.

Mesh independence, speed independence, turbulent layer height, and empirical correlation studies have been used to validate this model before extracting any data from each simulation.

There is simple model (*e.g., linear function*) for the relationship between inputs and output aerodynamic coefficients, mainly due to complex aerodynamic phenomena (flow separations, complex flow interactions). Therefore, aerodynamic coefficients need to be simulated at different attitudes. Given the available computing resources, even using mid-plane symmetry, the number of points that can be simulated is small. The following process has been developed:

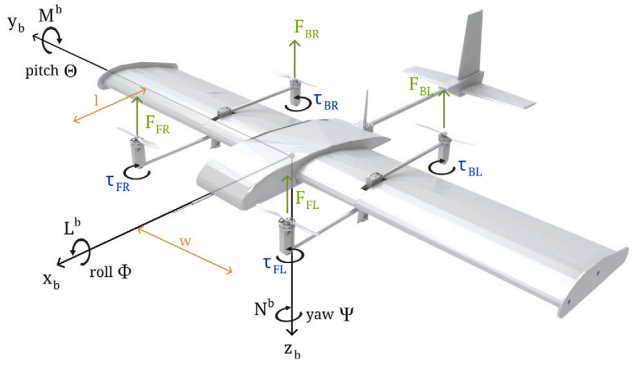

Fig. 3. Propulsive forces and moments diagram.

- In the first place, the domain has been subdivided into two different scenarios:
    1. **Controlled**: a region where the aircraft is assumed controllable, and therefore more precision is needed. Within angles $\phi \in [-9°, 12°]$, $\theta \in [-9°, 12°]$, $\psi \in [-180°, 180°]$. The limits for the roll and pitch values are defined by the region where the flight actions are considered safe and under control. Also, the typical aerodynamic parameters (such as C_L vs Angle of Attack slope) can be extracted from this region.
    2. **Uncontrolled**: for higher roll and pitch values, a loss of control is assumed, so the model does not require such high precision in terms of aerodynamic coefficients.
- For the controlled flight scenario, 100 points are simulated. A couple of hand-selected conditions are picked (48 points) to validate the CFD simulation technique: forward flight, tailwind, crosswind at 45, 90, and 135 degrees at different pitch and roll angles. The remaining 52 points are randomly generated within this range, using an algorithm that ensures a minimum predefined distance between each point.
- For the uncontrolled one, just a handful of points will be simulated. This calculation is only performed to ensure that the aerodynamic model follows real-world physics, so the flight controller understands when it has lost control and a crash is inevitable.
- Finally, to transform discrete simulations into a continuous model, a trilinear interpolation algorithm is proposed, allowing for data interpolation between the existing points.

4.1. CFD simulation setup

A crucial aspect in generating sufficient points for the discretization of every wind direction possible is assuring a proper distribution that thoroughly covers the desired range. First, 48 points are manually picked (in sets of 12) for various yaw angles: 0, 45, 90, 135, and 180 degrees, ranging from −9 to 12 degrees of pitch and roll in increments of 3. These points are manually selected to verify CFD data against actual available data.

Complex structures such as propeller-motor joints and carbon fiber arms have been neglected in the CFD simulation to facilitate convergence and ensure mesh quality. From experimental data, the simulated stall speed is approximately equal to the measured stall speed during flight, which shows that neglecting the motor supports and joints for aerodynamic purposes is a reasonable assumption.

Once CFD simulations have been correlated with real aerodynamic data, a simple algorithm generates random points (roll, pitch, and yaw) using a discrete uniform distribution [33].

Virtual wind tunnel speed is set to 9 m/s. The pressure-based solver is preferred for this type of slow flows. Since we are only looking for a specific set of coefficients, we do not need to study time-dependent solutions. Thus, we can go for a stationary simulation. Between the different solvers, the SIMPLE algorithm is preferable for this steady-state simulation. Heat and energy flux models can be deactivated. The calculated Reynolds number is $Re \approx 4 \cdot 10^5$, reflecting that we are facing a turbulent flow [34]. Inside RANS models, *k-omega SST* offers the best performance for this scenario:

- Two equation model: kinetic turbulent energy and dissipation.
- Wall functions
- Combination of *k-epsilon* for the outside boundary layer and outwards, and *k-omega* in the inner boundary layer.
- Suitable for separated flows and jet streams.
- Limited by difficulties to reach convergence.

A summary of the simulation parameters can be found in Table 1. The first layer height has been calculated to properly capture the viscous sublayer ($y^+ \approx 1$) [35]. After the complete simulation setup, mesh independence studies, and validation tests, a set of 100 different design points are simulated on ANSYS Fluent. Convergence is reached when residuals fall below a threshold of 10^{-6} [36].

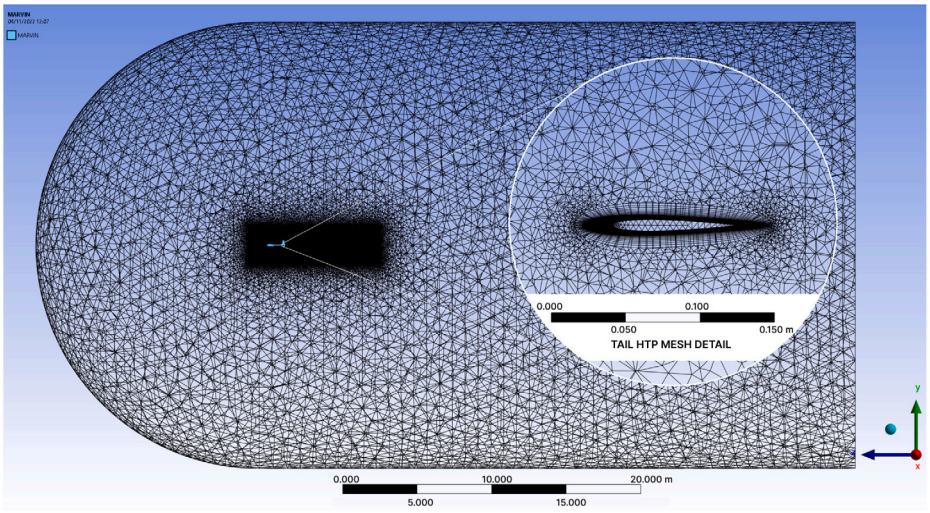

Fig. 4. Slice cut of the mesh, with HTP meshing detail.

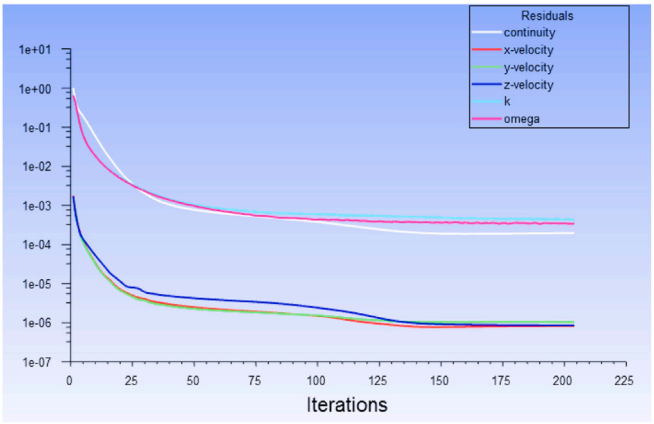

Fig. 5. Residuals plot screenshot from ANSYS for a simulation point.

An example of a residuals plot for a given attitude configuration can be seen in Fig. 5. The hybrid initialization method is chosen to accelerate convergence. Simulations are carried out in packs of 6 design points per run to free memory and review each set of points. Before each execution, all the simulation parameters including the mesh are verified using ANSYS Fluent's *Check Case* utility. A slice cut of a sample generated mesh can be seen in Fig. 4.

4.2. CFD simulation results

The result of these simulations is represented as an aerodynamic map containing C_L, C_D, C_Q, C_{LA}, C_{MA}, and C_{NA} values for each point in a range of roll ≈ 0 to simplify the visualization. Fig. 6 showcases the generated maps for the lift and drag coefficients. Fig. 7 shows the rest of the coefficients: lateral force, roll moment, yaw moment, and pitch moment. A visual analysis of the first two maps shows a strong dependence of lift and drag coefficients with the yaw and pitch angles, reaching optimal values at nose and tailwinds. Also, as expected, the lift coefficient is higher at front wind and higher pitch angles, while the drag coefficient is lower at lower pitch angles. The rest of the coefficients also show correspondence with reality. For example, the yaw moment coefficient is minimum when the aircraft is aligned with the wind, and maximum when it is perpendicular to it. Note that the roll angle is kept at 0 degrees in each of the six graphs.

Table 1
CFD simulation summary.

Parameter	Unit	Value
Wind tunnel speed	m/s	9
Estimated Re	–	4.00 e+05
Density	kg/m^3	1.225
Viscosity	kg/m s	1.7894e−05
Reference temperature	K	288.16
Reference length	m	1
Reference area	m^2	1
Average mesh nodes	–	4.65e+06
Average mesh cells	–	16.0e+06
First layer height	m	6.2e−05

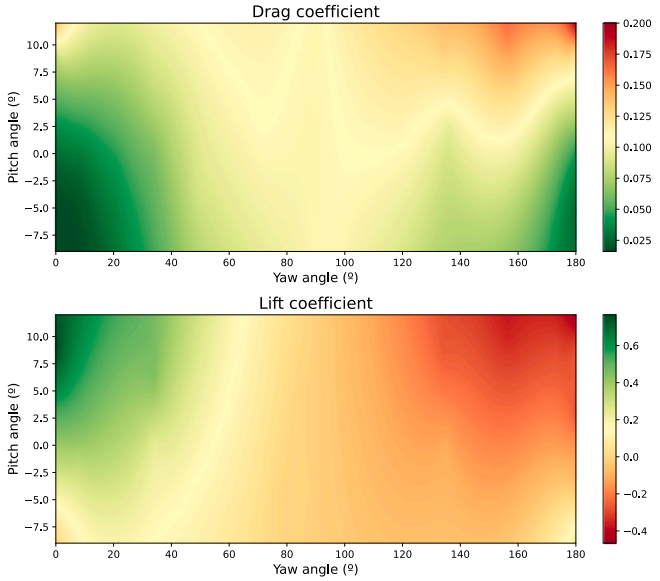

Fig. 6. Aerodynamic map of C_L and C_D for points with roll ≈ 0.

5. Software-in-the-loop flight controller

Once the physical model is complete, a flight controller must be implemented to recreate the UAV flight behavior. The actual Marvin aircraft runs a modified version of Ardupilot's open source flight controller software for VTOL aircrafts. Similarly, an instance of the modified Ardupilot[3] flight controller is executed in the same Linux computer that runs Gazebo. Communication between the UAV model in Gazebo and the flight controller is established via MAVLink [37]. Loading the parameters file of the actual UAV results in a complete Software-in-the-loop (SITL) solution.

A Taranis X9D+[4] is connected via USB to Ardupilot and setup as a joystick for pilot input.

6. VTOL-DT building

6.1. Model components

The VTOL-DT flight dynamics have been determined, and the aerodynamic coefficients have been characterized, but the rigid-body model has yet to be created in Gazebo. In order to reduce simulation times and improve overall training performance, the rigid body has been divided into the following components:

- **Fuselage**: .stl file containing the main body, wings and tail structure.
- **Motors** (x4): modeled in Gazebo as basic cylinders.

[3] https://ardupilot.org/.
[4] https://www.frsky-rc.com/product/taranis-x9d-plus-2/.

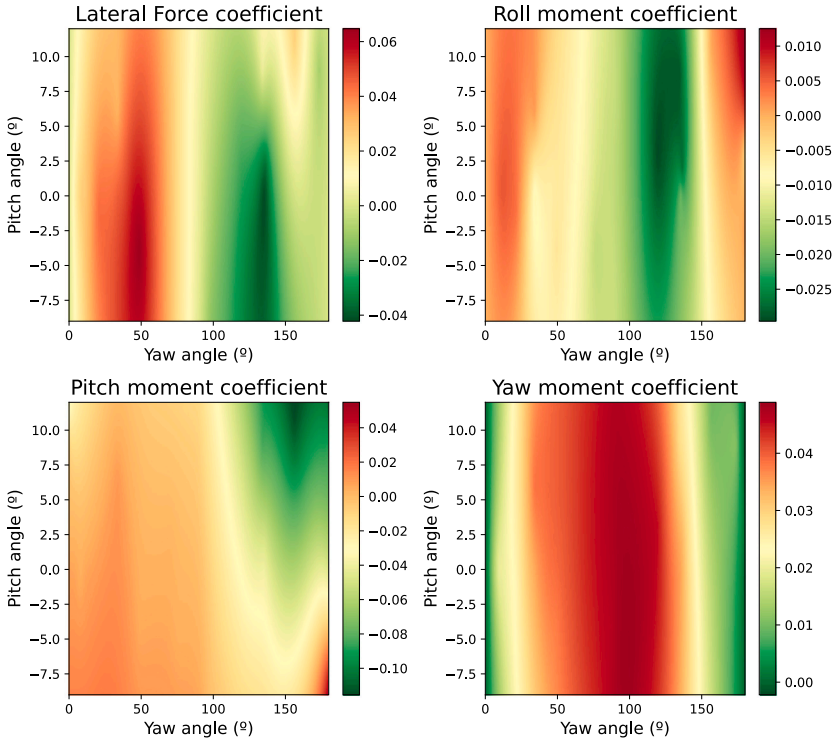

Fig. 7. Aerodynamic map of $C_{lateral}$, C_{roll}, C_{pitch}, and C_{yaw} for points with roll ≈ 0.

- **Propellers** (x4): modeled as flat sheets with the propellers' approximate size. Despite the different apparent shapes, aerodynamic and mass properties are carefully selected to model the physical propeller. Visually, the flat sheet is substituted by a 3D propeller design.
- **Arms** (x4): carbon rods connecting motors to the main fuselage. Again, they are modeled as simple cylinders with the appropriate mass properties.
- **Inertial Measurement Unit (IMU)**: introduced inside the fuselage, to gather attitude data for the training and simulation.

All the components have been included in the Gazebo model, and the origin of coordinates has been set at the Center of Mass of the aircraft (CoM). The next step is to assign mass and inertia properties to each component.

6.2. Moment of inertia, mass, and center of mass characterization

Various sources have been considered to estimate the moment of inertia and mass terms, as well as the center of mass for each component:

- **Component datasheets**: given by each manufacturer. Used to estimate the mass of propellers and motors.
- **Estimation**: a fully detailed 3D CAD model has been created in Solidworks[5] and Autodesk Inventor.[6] Internal modules allow for precise mass estimation, inertia values, and center of mass. Used for the body, arms, and motors.
- ***In situ* measurements**: components weighting to validate the two previous methods.

6.3. Wind plugin implementation

By implementing an interpolation algorithm, the generated points from Section 4 can be turned into a continuous function of roll, pitch, and yaw angles.

As already stated, Gazebo 11.0.0 includes an aerodynamic lift-drag plugin, but it is not suitable for this application, so a new aerodynamic plugin has been developed from scratch. This model takes 5 input values at any given instant and aircraft location:

[5] https://www.solidworks.com/.

[6] https://www.autodesk.es/products/inventor/.

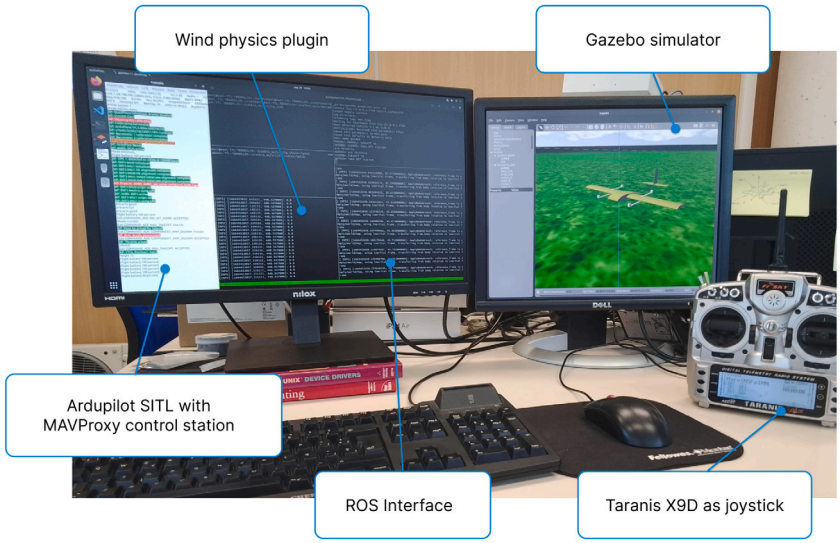

Fig. 8. Complete SITL simulator setup running.

- Aircraft attitude: roll (ϕ), pitch (θ), yaw (ψ).
- Atmospheric wind speed: $\vec{V}_{wind}$.
- Aircraft flight speed: $\vec{V}_{flight}$.

And outputs 6 values based on the atmospheric conditions and aircraft's mentioned properties:

- Forces acting on the center of gravity: L, D, Q.
- Moments acting on the center of gravity: M_A, L_A, N_A.

These aerodynamic forces and moments are then published via ROS to Gazebo, and added to the propulsive and gravity actions.

7. VTOL-DT testing

Once the simulation model described in Section 6.1 is compiled and loaded into Gazebo, we are left with a complete simulation setup as illustrated in Fig. 8.

Take-off, landing and hovering tests have been performed to evaluate the wind effect model against the conventional physics model in Gazebo. The exact same setup was employed in both scenarios. Attitude and motor outputs have been extracted from the SITL flight log and plotted in Figs. 9 and 10 for comparison. A flight simulation comparison video can be found in the link below.[7] For this test simulation, the following conditions have been set:

- Aircraft initially set to 0°: nose pointing to the north.
- Randomly selected wind direction of 15° coming from the northwest.
- Constant wind speed set to 6 m/s or 21.6 km/h, which is a typical caution threshold used by Marvin pilots during take-off. Windspeeds above this value are considered to be dangerous to take-off and land safely.
- Constant air density of 1.225 kg/m^3.
- All phases have been conducted automatically by the SITL flight controller. No pilot input has been used during this test.

Figs. 9 and 10 show the importance of including a wind physics model to predict the aircraft performance during take-off, landing and hovering.

The standard physics model shows a nearly perfect flight, where the attitude is almost unaffected and motor response is very stable and equal for all the motors. In contrast, when the wind model is applied heavy oscillations can be seen in attitude due to the flight controller trying to maintain control against the wind. The motor response also features these oscillations, showing different output speeds for the front and rear motors, which is a very important performance aspect. Two motors are constantly pushed to more than 80% of their maximum output, indicating that slightly higher wind speeds would cause motor saturation and invoke a high risk situation for the pilot. This proves why the usual take-off limit wind speed is set to 6 m/s in standard Marvin operations.

After evaluating the custom wind physics model in simulation, flight test experiments in real wind conditions have been conducted following the listed procedure:

[7] Flight simulation videos: https://youtu.be/2rvquHHQDS8.

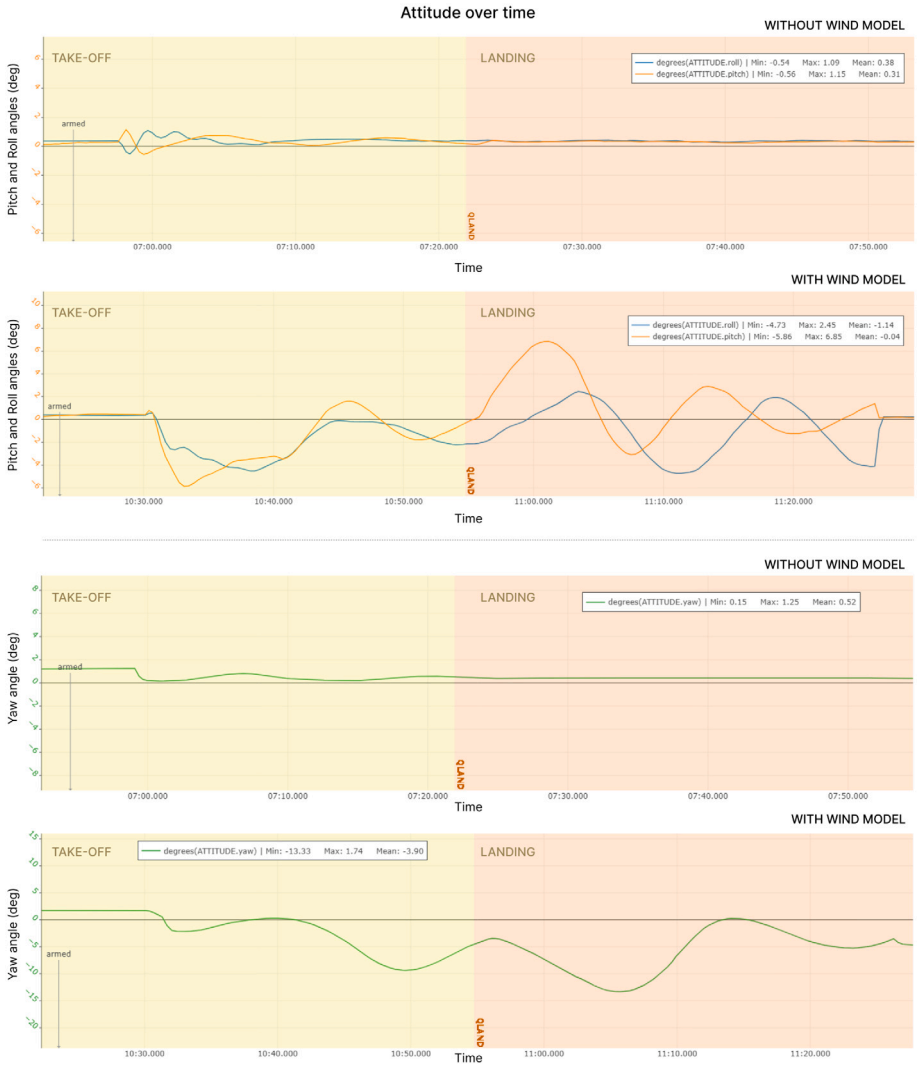

Fig. 9. Comparison plot of attitude angles (roll, pitch & yaw) using a conventional physics model and our custom wind model during take-off, short hovering and landing.

1. The UAV is placed at ground level with a fully charged battery. The IMU is calibrated for a stable level flight.
2. Wind conditions are measured and averaged during the experimental run at an approximate height of 2 meters to avoid ground-proximity effects.
3. The aircraft is taken off manually and switched to a position hold mode.
4. Once the position is fixed despite the wind, the aircraft is switched to a stabilized mode and the pilot sticks are liberated.
5. The aircraft is freely drafted by the wind. The pilot is only responsible for recovering control after a certain period of time or aircraft displacement.

Note that due to the available wind measuring instrumental, only average wind speed and direction values have been collected during experimental flights. Therefore, only the average wind components can be considered in simulation, even though the simulator is perfectly capable of reproducing any provided input.

In total, more than 15 min of flight data were analyzed from experimental flights to validate the simulation. From the recorded data, 4 test cases have been selected and reproduced from the multiple runs in the simulator to validate the Digital-Twin's wind physics, as noted in Table 2. The results can be seen in the linked video.[8]

[8] Flight experiment videos: https://youtu.be/2BMcp3AFbRE.

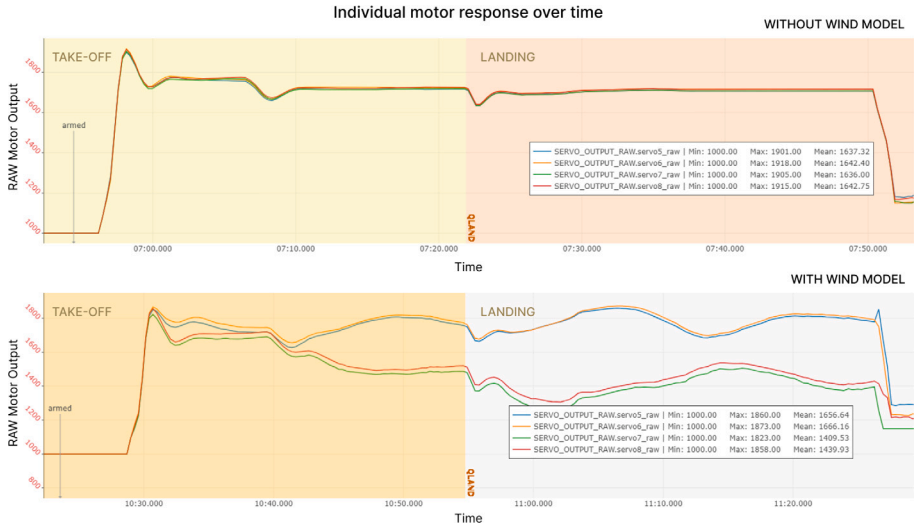

Fig. 10. Comparison plot of individual motor responses using a conventional physics model and our custom wind model during take-off, short hovering and landing.

Table 2
Flight test selected cases.

Case	Initial yaw (°)	Wind direction (°)	Windspeed (m/s)
1	318	330	5
2	289	344	4.5
3	340	330	6
4	340	350	5

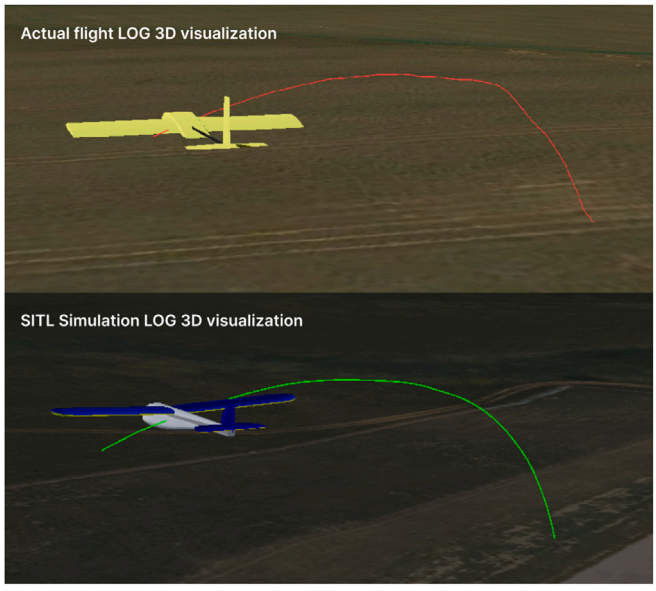

Fig. 11. Comparison of the 3D trajectory followed by the UAV in real wind conditions (above) and simulated wind conditions (below) for the second case.

7.1. Results

The UAV is drafted following a similar 3D trajectory in all four cases. For reference, Figs. 11 and 12 show the 3D visualization of two trajectories followed by the actual UAV and the simulated UAV respectively. Trajectories are extracted from the flight logs in both cases. The night scene in the simulated flight log is just caused by the Ardupilot SITL timezone not being configured.

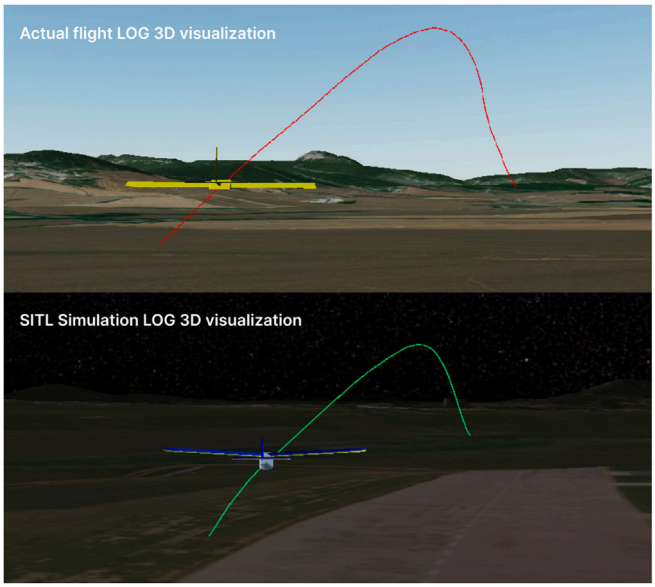

Fig. 12. Comparison of the 3D trajectory followed by the UAV in real wind conditions (above) and simulated wind conditions (below) for the fourth case.

Initially, when the relative speed to the wind is at its highest, the aerodynamic forces are maximum and, therefore, the acceleration is maximum. As a result, the aircraft is lifted and accelerated in the wind direction. Once the VTOL reaches the wind speed, the aerodynamic forces tend to zero, reducing the amount of lift produced and decreasing the height. There is no opposing force to the drag-induced speed, so the horizontal displacement is maintained at approximately the wind speed.

Aerodynamic moments are canceled out both in the real world and the simulation by the flight controller, so the effects are negligible.

The aircraft has been accurately described in simulation based on its actual physical properties. The flight controller runs the exact same configuration and code both in simulation and real flight, and the propulsive subsystem has been modeled to accurately mimic the real behavior from exhaustive motor bench tests. Therefore, most differences between both scenarios come from the way the wind has been modeled in the simulation. The available wind measuring equipment only provided mean wind speed and direction values. Thus, the wind can only be modeled based on the mean intensity and direction, omitting the fluctuations caused by turbulence. Due to this, comparing the variations in the aircraft's attitude does not provide any valuable information since most of the oscillations come from wind turbulence.

In general terms, the simulation strongly correlates with the actual flight experiments, proving that the aerodynamic model is working as expected. For better reference, readers are encouraged to watch the linked video.

8. Conclusion

Throughout this paper, we have successfully created and tested the digital twin of a custom commercial VTOL convertiplane UAV in copter mode in Gazebo.

Starting from *Euler's motion equations for rigid body dynamics*, we have developed a novel mathematical model that takes into account wind blowing from any possible direction to obtain the corresponding aerodynamic forces and moments. More than 100 CFD simulations have been carried out to discretize the dependence of aerodynamic coefficients on the incoming wind direction.

This novel approach will allow for VTOL convertiplane UAVs to be trained and tested in take-off, hovering, and landing maneuvers without the hassle of physical testing and dependence on existing wind conditions.

The model has performed as expected in all the experiments, with realistic-looking results and close to actual physical behaviors in every tested scenario. Most limitations have come from the way the wind was captured during experimental flights, limiting the ability to reproduce wind gusts and turbulence in simulation.

Future work includes developing precision equipment to capture instantaneous wind speed and direction. With the appropriate measuring tools wind could be exactly reproduced in simulation, capturing turbulence effects and achieving an even more realistic performance.

Declaration of competing interest

The authors declare that they have no known competing financial interests or personal relationships that could have appeared to influence the work reported in this paper.

Data availability

The authors do not have permission to share data.

Acknowledgment

The authors would like to thank Asociación Club Navarra de Aeromodelismo (ACNA) for granting us access to their facilities for conducting flight tests. Open access funding provided by Universidad Pública de Navarra.

Appendix A. Supplementary data

Supplementary material related to this article can be found online at https://doi.org/10.1016/j.simpat.2022.102703.

References

[1] S. Jordan, J. Moore, S. Hovet, J. Box, J. Perry, K. Kirsche, D. Lewis, Z.T.H. Tse, State-of-the-art technologies for UAV inspections, IET Radar, Sonar Navig. 12 (2) (2018) 151–164, http://dx.doi.org/10.1049/iet-rsn.2017.0251, arXiv:https://ietresearch.onlinelibrary.wiley.com/doi/pdf/10.1049/iet-rsn.2017.0251, URL https://ietresearch.onlinelibrary.wiley.com/doi/abs/10.1049/iet-rsn.2017.0251.
[2] A. Vuruskan, B. Yuksek, U. Ozdemir, A. Yukselen, G. Inalhan, Dynamic modeling of a fixed-wing VTOL UAV, in: 2014 International Conference on Unmanned Aircraft Systems (ICUAS), 2014, pp. 483–491, http://dx.doi.org/10.1109/ICUAS.2014.6842289.
[3] R. Clothier, R. Walker, Determination and evaluation of UAV safety objectives, in: S. Hugo (Ed.), Proceedings of the 21st International Conference on Unmanned Air Vehicle Systems, University of Bristol, United Kingdom, 2006, pp. 18.1–18.16, URL https://eprints.qut.edu.au/4183/.
[4] M. Grieves, Digital twin: Manufacturing excellence through virtual factory replication, 2015.
[5] M. Chetan, S. Yao, D.T. Griffith, Multi-fidelity digital twin structural model for a sub-scale downwind wind turbine rotor blade, Wind Energy 24 (12) (2021) 1368–1387, http://dx.doi.org/10.1002/we.2636, arXiv:https://onlinelibrary.wiley.com/doi/pdf/10.1002/we.2636, URL https://onlinelibrary.wiley.com/doi/abs/10.1002/we.2636.
[6] L. Wright, S. Davidson, How to tell the difference between a model and a digital twin, Adv. Model. Simul. Eng. Sci. 7 (1) (2020) 1–13.
[7] M. Bacic, On hardware-in-the-loop simulation, in: Proceedings of the 44th IEEE Conference on Decision and Control, 2005, pp. 3194–3198, http://dx.doi.org/10.1109/CDC.2005.1582653.
[8] R. Isermann, J. Schaffnit, S. Sinsel, Hardware-in-the-loop simulation for the design and testing of engine-control systems, Control Eng. Pract. 7 (5) (1999) 643–653, http://dx.doi.org/10.1016/S0967-0661(98)00205-6, URL https://www.sciencedirect.com/science/article/pii/S0967066198002056.
[9] M. Shafto, M. Conroy, R. Doyle, E. Glaessgen, C. Kemp, J. LeMoigne, L. Wang, Modeling, simulation, information technology & processing roadmap, Natl. Aeronaut. Space Adm. 32 (2012) 1–38.
[10] C.-s. Yoo, Y.-s. Kang, B.-j. Park, Hardware-In-the-Loop simulation test for actuator control system of Smart UAV, in: ICCAS 2010, 2010, pp. 1729–1732, http://dx.doi.org/10.1109/ICCAS.2010.5669783.
[11] J. Sun, B. Li, C.-Y. Wen, C.-K. Chen, Design and implementation of a real-time hardware-in-the-loop testing platform for a dual-rotor tail-sitter unmanned aerial vehicle, Mechatronics 56 (2018) 1–15, http://dx.doi.org/10.1016/j.mechatronics.2018.10.001, URL https://www.sciencedirect.com/science/article/pii/S0957415818301521.
[12] M.B. Ayed, L. Zouari, M. Abid, Software in the loop simulation for robot manipulators, Eng., Technol. Appl. Sci. Res. 7 (5) (2017).
[13] y. Magnussen, G. Hovland, M. Ottestad, Multicopter UAV design optimization, in: 2014 IEEE/ASME 10th International Conference on Mechatronic and Embedded Systems and Applications (MESA), 2014, pp. 1–6, http://dx.doi.org/10.1109/MESA.2014.6935598.
[14] Y. Yang, W. Meng, S. Zhu, A digital twin simulation platform for multi-rotor UAV, in: 2020 7th International Conference on Information, Cybernetics, and Computational Social Systems (ICCSS), 2020, pp. 591–596, http://dx.doi.org/10.1109/ICCSS52145.2020.9336872.
[15] A. Rassõlkin, V. Rjabtšikov, T. Vaimann, A. Kallaste, V. Kuts, A. Partyshev, Digital twin of an electrical motor based on empirical performance model, in: 2020 XI International Conference on Electrical Power Drive Systems (ICEPDS), IEEE, 2020, pp. 1–4.
[16] K. Yan, W. Xu, B. Yao, Z. Zhou, D.T. Pham, Digital twin-based energy modeling of industrial robots, in: Asian Simulation Conference, Springer, 2018, pp. 333–348.
[17] N. Kousi, C. Gkournelos, S. Aivaliotis, C. Giannoulis, G. Michalos, S. Makris, Digital twin for adaptation of robots' behavior in flexible robotic assembly lines, Procedia Manuf. 28 (2019) 121–126.
[18] R. Bansal, M.A. Khanesar, D. Branson, Ant colony optimization algorithm for industrial robot programming in a digital twin, in: 2019 25th International Conference on Automation and Computing (ICAC), IEEE, 2019, pp. 1–5.
[19] P. Stączek, J. Pizoń, W. Danilczuk, A. Gola, A digital twin approach for the improvement of an autonomous mobile robots (AMR's) operating environment—A case study, Sensors 21 (23) (2021) 7830.
[20] Gazebo, Tutorial: Using Gazebo plugins with ROS, 2014, URL http://gazebosim.org/tutorials?tut=ros_gzplugins.
[21] S. Shah, D. Dey, C. Lovett, A. Kapoor, Airsim: High-fidelity visual and physical simulation for autonomous vehicles, in: Field and Service Robotics, Springer, 2018, pp. 621–635.
[22] S. Documentation, Simulation and model-based design, 2020, URL https://www.mathworks.com/products/simulink.html.
[23] J. Haas, A history of the unity game engine, Diss, Worcester Polytechnic Institute, 2014.
[24] N.R. Council, et al., Low-Altitude Wind Shear and Its Hazard To Aviation, National Academies Press, 1983.
[25] A. Chakrabarty, J. Langelaan, UAV flight path planning in time varying complex wind-fields, in: 2013 American Control Conference, 2013, pp. 2568–2574, http://dx.doi.org/10.1109/ACC.2013.6580221.
[26] D.E. Raveh, CFD-based models of aerodynamic gust response, J. Aircr. 44 (3) (2007) 888–897.
[27] A. Brezoescu, P. Castillo, R. Lozano, Wind estimation for accurate airplane path following applications, J. Intell. Robot. Syst. 73 (1) (2014) 823–831.
[28] L. Lei, G. Shen, L. Zhang, Z. Li, Toward intelligent cooperation of UAV swarms: When machine learning meets digital twin, IEEE Netw. 35 (1) (2021) 386–392, http://dx.doi.org/10.1109/MNET.011.2000388.
[29] M.Á.G. Tierno, M.P. Cortés, C.P. Márquez, Mecánica Del Vuelo, Ibergaceta, 2012.
[30] E.L. Duke, R.F. Antoniewicz, K.D. Krambeer, Derivation and Definition of a Linear Aircraft Model, Vol. 1207, National Aeronautics and Space Administration, Scientific and Technical ..., 1988.
[31] T. Luukkonen, Modelling and control of quadcopter, Indep. Res. Proj. Appl. Math., Espoo 22 (2011) 22.
[32] H. Merabti, I. Bouchachi, K. Belarbi, Nonlinear model predictive control of quadcopter, in: 2015 16th International Conference on Sciences and Techniques of Automatic Control and Computer Engineering (STA), 2015, pp. 208–211, http://dx.doi.org/10.1109/STA.2015.7505151.
[33] P.H. Westfall, R.D. Wolfinger, Multiple tests with discrete distributions, Amer. Statist. 51 (1) (1997) 3–8.

[34] K.T. Trinh, On the critical Reynolds number for transition from laminar to turbulent flow, 2010, arXiv preprint arXiv:1007.0810.
[35] S.M. Salim, S. Cheah, Wall Y+ strategy for dealing with wall-bounded turbulent flows, in: Proceedings of the International Multiconference of Engineers and Computer Scientists, Vol. 2, 2009, pp. 2165–2170.
[36] J. Tu, G.H. Yeoh, C. Liu, Computational Fluid Dynamics: A Practical Approach, Butterworth-Heinemann, 2018.
[37] A. Koubâa, A. Allouch, M. Alajlan, Y. Javed, A. Belghith, M. Khalgui, Micro air vehicle link (mavlink) in a nutshell: A survey, IEEE Access 7 (2019) 87658–87680.